Spectroscopic signatures of domain walls in hexagonal ErMnO_{3}

Q.-C. Sun, Xiaoxiang Xi, X. Wang, N. Lee, D. Mazumdar, R. J. Smith, G. L. Carr, S.-W. Cheong, and J. L. Musfeldt

Spectroscopic Signatures of Domain Walls in Hexagonal ErMnO$_3$

Q. -C. Sun†,^{1} Xiaoxiang Xi,^{2} N. Lee$^{\perp}$,^{3} D. Mazumdar,^{1} R. J. Smith,^{2} G. L. Carr,^{2} S. -W. Cheong,^{3} and J. L. Musfeldt^1

^{1}Department of Chemistry, University of Tennessee, Knoxville, Tennessee 37996, USA
^{2}Photon Sciences, Brookhaven National Laboratory, Upton, New York 11973, USA
^{3}Rutgers Center for Emergent Materials and Department of Physics and Astronomy,
Rutgers University, Piscataway, New Jersey 08854, USA

We measured the spectroscopic response of stripe- and vortex-containing ErMnO$_3$ in order to uncover the electronic properties of the domain walls. We quantify Born effective charge and polarization differences using the lattice behavior, analyze the local rare earth environment from the f-manifold excitations, and reveal how shifts in the charge transfer excitations impact the band gap. The increased Born charge, polarization, and band gap in the vortex-containing material are brought together with a discussion of hybridization and wall density effects.

Domain walls are fascinating. In multiferroics like BiFeO$_3$, they appear in a variety of patterns, are both insulating and conducting, and can be rearranged by external stimuli like electric field and strain [1, 2]. Recently, domain walls were discovered in hexagonal rare earth manganites (RMnO$_3$, R = rare earth) [3–11], where they take on either stripe or Z2 × Z3 vortex patterns depending upon the growth temperature and whether the crystals are cooled slowly or quenched (Fig. 1(a,b)) [7, 10, 11]. These patterns have been imaged by a variety of techniques [4–12] and reveal that stripe-containing crystals have linear domain walls whereas vortex-containing samples have six unique walls merged at a point [13]. The topological defect configuration is characterized by Mn^{3+} trimerization, which emanates from successive MnO$_5$ tilting around three different origins, combined with vortex vs. antivortex domain walls that arise from "in" and "out" tilting orientations [4, 10, 14–16]. This process induces the structural instability that leads to ferroelectricity [3, 14, 17, 18]. Hexagonal ErMnO$_3$ attracted our attention as a system with which to investigate the spectroscopic signatures of domain walls. This rare earth manganite is ferroelectric below T$_C$ = 1150 °C, antiferromagnetic below T$_N$ = 81 K, and forms switchable stripe and vortex domain structures [7, 10, 11, 19, 20].

In this Letter, we report the electrodynamic response of domain walls in ErMnO$_3$. By comparing two crystals with very different domain wall concentrations, we are, for the first time, able to investigate the spectroscopic characteristics of these structures. The vibrational response of the vortex-containing ErMnO$_3$ reveals an increase in Born effective charge that is directly related to the ferroelectric polarization. We argue that this difference is a combined density and hybridization effect, the latter of which emanates from the modified local structure of the domain walls as compared to the bulk. Moreover, the f-manifold excitations display intensity variations that are consistent with decreasing hybridization and splitting that indicates the local Er environment is unaffected by the presence of walls. Finally, the blue

shifted electronic excitations in the vortex crystal are discussed in terms of a slightly modified crystal field environment around the Mn centers, a band gap that increases from 2.5 to 3.1 eV, and significantly reduced hybridization effects. These findings are important for understanding the influence of structural domain walls on the electronic properties of multiferroics like hexagonal ErMnO$_3$ and other multifunctional oxides that contain metastable domain walls [21, 22].

High quality single crystals of hexagonal ErMnO$_3$ were grown by flux techniques [23]. The platelets have large ab-plane faces, with c perpendicular to the surface. These crystals are well characterized by us and other teams [12, 24]. The thermal sequence, which controls the number of domain walls, is detailed in Ref. [24]. Domain wall density in the vortex sample is clearly much greater
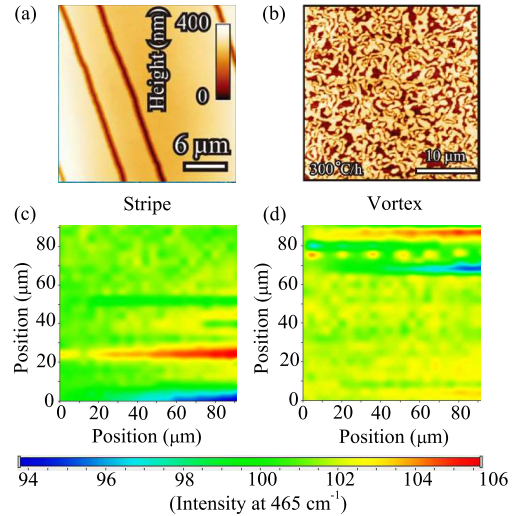

FIG. 1: (a,b) Atomic force microscope images of chemically-etched ErMnO$_3$ with stripe and vortex domain wall patterns [7]. (c,d) Real space micro-reflectance mapping of stripe- and vortex-containing ErMnO$_3$ at 465 cm^{-1}. The strong red and blue streaks are due to synchrotron injection cycles.

than that in the stripe crystal (Fig. 1(a, b)). We estimate ≈200 and 10^6 domain walls/mm³ for stripe and vortex, respectively [25]. Transmittance and near normal reflectance were measured using a Bruker 113V Fourier transform infrared spectrometer, an Equinox 55 Fourier transform instrument (equipped with a microscope attachment), and a Perkin Elmer λ-900 grating spectrometer. The optical constants were determined using combined Glover-Tinkham and Kramers-Kronig techniques. Real space infrared imaging was carried out at the U12IR beamline at the National Synchrotron Light Source using a Spectra-Tech Irμs infrared microspectrometer with a programmable motorized mapping stage. We mapped a 90×90 μm² area between 380 and 5000 cm⁻¹ in reflectance mode with a 3 μm step size and a 24×18 μm² spot size. Infrared contrast is shown at 465 cm⁻¹.

Figure 2(a) displays the 300 K infrared reflectance of stripe and vortex ErMnO₃ in the ab plane. There are six infrared-active E₁ symmetry vibrational modes [26]. Table I summarizes the displacement patterns. Taking the response of the stripe-containing crystal to be our control [25], we extract the vibrational signature of the domain walls in isolation from a difference calculation: $\Delta R = R_{vortex} - R_{stripe} = R_{wall}$ (Fig. 2(b)). To understand this contrast, we calculated the optical constants using a Kramers-Kronig analysis. Figure 2(c) displays the optical conductivity of the stripe- and vortex containing crystals. They are overall similar in character, with identical transverse optic (TO) phonon frequencies (Table I), befitting the shared hexagonal structures that differ only in topology [4, 6] and typical of systems in which the oxygen content is identical and under control. The conductivity difference spectrum $\Delta \sigma_1 = \sigma_{1,vortex} - \sigma_{1,stripe} = \sigma_{1,wall}$ is again a measure of the domain wall response (Fig. 2(d)). The fact that the reflectance and conductivity differences are quite similar argues for a dissipative rather than underlying dielectric constant effect. The main variation is in the vicinity of the phonon modes, with features that involve apical oxygen (O$_A$) motion [26] showing the most pronounced intensity changes. This is because apical oxygen displacement is associated with MnO₅ tilting. The phonon intensity variations are also apparent in the partial sum rule, from which we see that the vortex-containing sample has additional oscillator strength.

But where does the extra oscillator strength in the more highly textured crystal come from, and what does it reveal about the electronic properties? In the following, we argue that it arises due to a decrease in hybridization. We quantify the phonon contrast with a partial sum rule calculation in which the effective number of electrons involved in these excitations, N_{eff}, is a sum over the frequency dependent optical conductivity:
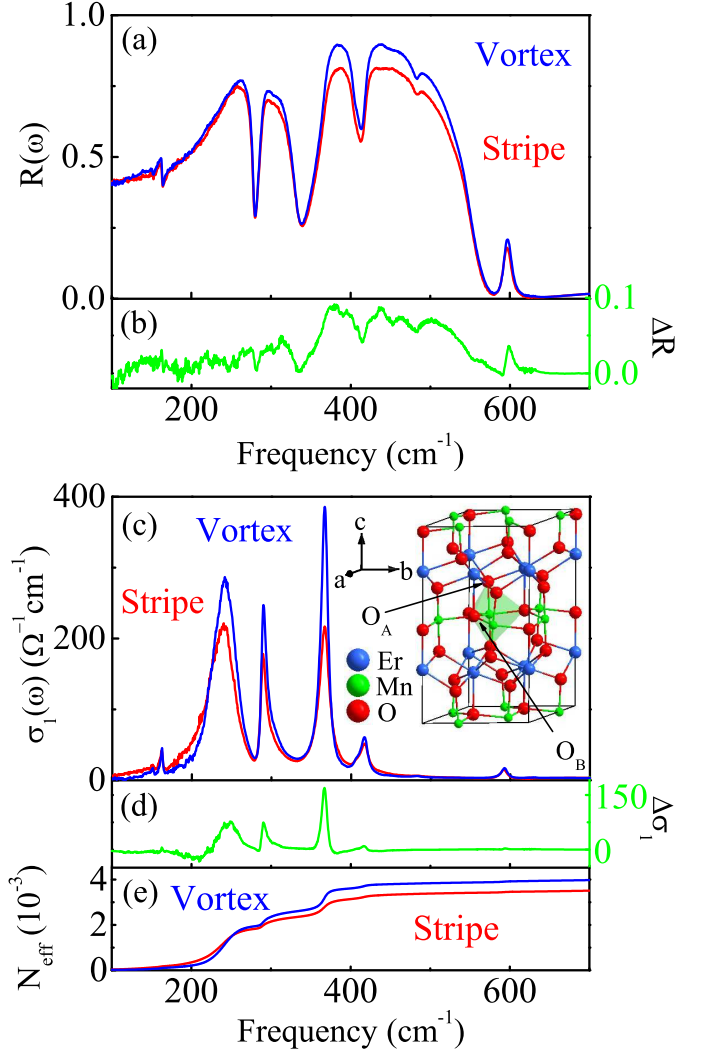

FIG. 2: (a) Close-up view of the reflectance spectra of stripe- and vortex-containing ErMnO₃ at 300 K [7]. (b) Reflectance difference spectrum: $\Delta R = R_{vortex} - R_{stripe}$. (c) 300 K optical conductivity of stripe and vortex samples. Inset: crystal structure of ErMnO₃ [27]. The unit cell is hexagonal ($a = 6.1121$ Å and $c/a=1.8684$ at 300 K), with 6 formula units and a $P6_3cm$ space group. O$_A$ and O$_B$ refer to the apical and basal plane oxygens of the triangular bipyramidal cages, respectively. (d) Optical conductivity difference spectrum: $\Delta \sigma_1 = \sigma_{1,vortex} - \sigma_{1,stripe}$. (e) Effective number of electrons involved in the excitations, N_{eff}, as a function of frequency.

$$N_{eff}(\omega) = \int_{\omega_1}^{\omega_2} \frac{2\sigma_1(\omega)}{\pi \epsilon_0 \omega_p^2} d\omega. \tag{1}$$

Here, $\omega_p = \sqrt{e^2/V m_e \epsilon_0}$ is the plasma frequency, e and m_e are the charge and mass of an electron, ϵ_0 is the permittivity of free space, V is the unit cell volume, and ω_1 and ω_2 are the frequency limits of integration. Figure 2(e) shows that N_{eff} starts to grow above 160 cm⁻¹ where the first E₁ symmetry mode begins to contribute.

TABLE I: Summary of infrared-active vibrational modes in ErMnO$_3$: symmetries, a brief description of displacement patterns, transverse optic (TO) phonon frequencies, and oscillator strengths (S_j). Here, O$_A$ and O$_B$ refer to the apical and the basal plane oxygens of the triangular bipyramidal cages as shown in inset of Fig. 2 [26]. That the TO frequencies are the same is good evidence that the oxygen content is identical.

Mode	Main atomic displacements	Stripe TO (cm^{-1})	S_j	Vortex TO (cm^{-1})	S_j
E$_1$	a,b (Er)	162.3	0.35	162.3	0.41
E$_1$	a,b (O$_A$) -a,b (O$_B$,Mn)	241.2	6.84	241.2	7.60
E$_1$	a,b (O$_A$)	290.0	1.54	290.0	1.95
E$_1$	a,b (O$_B$) -a,b (O$_A$,Mn)	366.8	1.40	366.8	1.72
E$_1$	a,b (O$_B$,O$_A$) -a,b (Mn)	417.6	0.261	417.6	0.286
E$_1$	a,b (O$_B$)	592.8	0.134	592.8	0.144

The effective number of electrons participating in these excitations increases with frequency, with strong phonons contributing more to N_{eff} than smaller structures. To qualify the oscillator strength (S_j) of each mode, we evaluated the area under each peak in $\sigma_1(\omega)$. As shown in Table I, mode strengths in the vortex-containing crystal are larger than those in the stripe-containing material. The optical conductivity difference (Fig. 2(b)), which we have argued represents the lossy signature of the domain walls rather than a simple static dielectric effect, can therefore be interpreted as a change in the oscillator strength: $\frac{\int \Delta\sigma_{1,j}}{\int \sigma_{1,stripe,j}} \sim \frac{\Delta S_j}{S_{stripe,j}}$. Here, $\Delta\sigma_1$ is defined as before and $\Delta S_j = S_{vortex,j} - S_{stripe,j}$, where j is the mode index.

With these optical constants, we evaluate the chemical bonding by calculating Born effective charges as [28]:

$$4\pi^2 c^2 \sum_j \omega_{TO,j}^2 \cdot S_j = \frac{Ce^2}{\epsilon_0 V} \sum_k \frac{(Z_{B,k}^*)^2}{m_k}. \quad (2)$$

Here, Z_{Bk}^* is the Born effective charge on the k-th ion, C is the number of formula units in the unit cell, m_k is the atomic mass of the k-th atom. This analysis yields a striking result (Table II). The Born effective charge for the Er and Mn centers increases from 3.08 e in the control sample containing only a few stripes to 3.32 e in the vortex sample which contains many domain walls - an 8% contrast. The presence of structural domain walls leads to differences in chemical bonding around the Er and Mn centers. Ferroelectric polarization is given by $P = \frac{e}{V} \sum_k Z_{B,k}^* u_k$, where u_k is the ionic displacement of the k-th center [28]. Assuming similar displacement patterns, the Born charge difference in ErMnO$_3$ translates into a change in ferroelectric polarization: $\frac{\Delta Z_B^*}{Z_{B,stripe}} = \frac{\Delta P}{P_{stripe}}$ = 8%, where $\Delta Z_B^* = Z_{B,vortex}^* - Z_{B,stripe}^*$ and $\Delta P = P_{vortex} - P_{stripe}$. Using rough estimates of domain wall

TABLE II: Summary of Born effective charge (Z_B^*) in both materials for $\vec{E} \perp c$ along with the change in this quantity.

Born effective charge	Stripe (e)	Vortex (e)	Difference
Z_B^* (Er or Mn center)	3.08	3.32	$\frac{\Delta Z_B^*}{Z_{B,stripe}^*} = 8\%$
Z_B^* (O center)	-2.06	-2.22	

densities [25], we project that a domain wall contributes about 10^{-5} % to the polarization. As a consistency check, we also analyzed the Born charge of the O centers. We find -2.06 e and -2.22 e for the stripe and vortex sample, respectively (Table II). The larger Born effective charge of the vortex sample indicates that walls make ErMnO$_3$ more ionic, consistent with recent predictions [15].

To better understand the connection between domain density, Born charge, and ferroelectric polarization, we scanned the infrared reflectance at 465 cm^{-1}, a process that allowed us to create real space images and visualize charge contrast (Fig. 1(c,d)). The purpose was not to replicate the real space images from atomic force microscopy, but to find the signatures of ferroelectric lattice distortion emanating from the domain structures. Although the technique lacks the necessary resolution, the scans show higher intensity in the vortex crystal at 465 cm^{-1} than in the stripe-containing sample, consistent with the enhanced phonon intensities discussed above.

Figure 3(a) displays the near infrared absorption spectrum of stripe and vortex ErMnO$_3$. Two clusters near 0.8 and 1.3 eV are apparent. We assign these features as f manifold excitations, activated by spin-orbit coupling [20, 29] and the Stark effect, the latter of which is
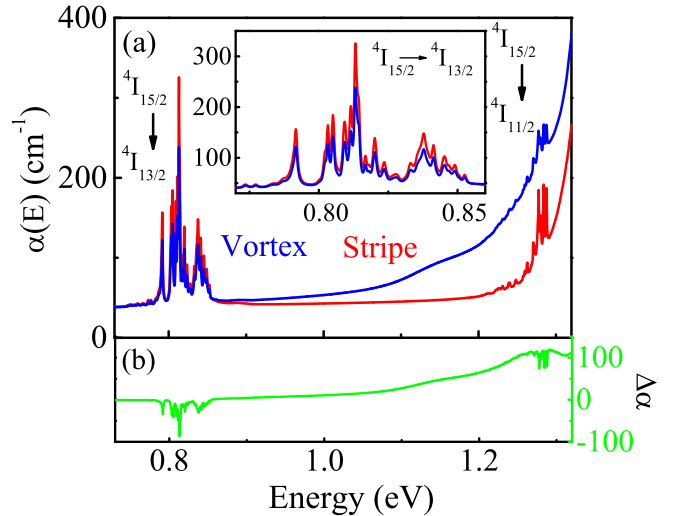

FIG. 3: (a) ab plane absorption spectrum of stripe and vortex ErMnO$_3$. Inset: close-up of the ^{4}I$_{15/2}$ → ^{4}I$_{13/2}$ cluster, showing a 1:1 correspondence of peak positions but clear intensity differences. (b) Absorption difference spectrum, $\Delta\alpha = \alpha_{vortex} - \alpha_{stripe} = \alpha_{wall}$, in the range of the f manifold transitions and leading edge of the Mn on-site excitation.

a consequence of the thermal population of higher Stark levels in the $^4I_{15/2}$ ground state [20, 29]. The cluster at ≈ 0.8 eV is assigned to $^4I_{15/2} \rightarrow {}^4I_{13/2}$ excitations, and the peaks at ≈ 1.3 eV are associated with $^4I_{15/2} \rightarrow {}^4I_{11/2}$ excitations. A close-up view of the ground $^4I_{15/2}$ state $\rightarrow$ first excited $^4I_{13/2}$ state features (inset, Fig. 3(a)) shows that the peak pattern is exactly the same in both samples, right down to the last detail. This striking result reveals that the Er environment is identical in the stripe- and vortex-containing crystals - at least at room temperature. We can understand this finding by realizing that spin-orbit coupling is much larger than crystal field splitting in a rare earth center, so the local environment is insensitive to domain formation [29].

At the same time, the absorption difference spectrum $\Delta\alpha = \alpha_{vortex} - \alpha_{stripe} = \alpha_{wall}$ uncovers intensity variations in the f-manifold excitations (Fig. 3(b)). Fermi's golden rule advances a mechanism by which f manifold transition intensities can depend upon wall density [30]:

$$W_{i \rightarrow f} = \frac{2\pi}{\hbar} \mid M \mid^2 g(\hbar\omega). \qquad (3)$$

Here, $W_{i \rightarrow f}$ is the transition rate for excitation from an initial state ψ_i to final state ψ_f by absorption of a photon ($\hbar\omega$), and M is the matrix element given by $M = \int \psi_f^*(r) H'(r)\psi_i(r)d^3r$ where H' is the perturbation, r is the position vector of the electron, and $g(\hbar\omega)$ is the density of states. The large number of structurally distorted domain walls in the vortex-containing crystal decreases the matrix element and reduces hybridization, an effect made manifest as diminished f manifold transition intensities. This finding is consistent with a higher Born charge in the vortex-containing crystal.

Figure 4(a) displays the optical response of ErMnO$_3$. Based upon first principles electronic structure calculations on TbMnO$_3$ [31, 32] and prior spectroscopic work on LuMnO$_3$ and other rare earth manganites [32, 33], we assign these features to a combination of Mn $d \rightarrow d$ on-site and O $p \rightarrow$ Mn d charge transfer excitations. With the exception of the leading edge of the 1.55 eV absorption band (right hand side, Fig. 3(a)), all features blue shift in the vortex-containing crystal compared to those in the stripe-containing sample. The O $p \rightarrow$ Mn d charge transfer excitations above 2.5 eV are especially sensitive to this effect [34]. We attribute the blue shift to a decrease in hybridization in the vortex crystal.

We estimate the crystal field splitting of Mn in a trigonal bipyramidal environment from the position of the on-site excitation (inset, Fig. 4) [35]. We find $10Dq = 1.52$ and 1.54 eV for the stripe and vortex samples, respectively. These estimates compare well with the value found in LuMnO$_3$ (10Dq = 1.7 eV) [33]. The difference, $\Delta 10Dq = 0.02$ eV (160 cm^{-1}), is small compared to the electrostatic interaction parameter for Mn^{3+} ($B = 1140$ cm^{-1}) [35]. Wall density has only a modest effect on the Mn crystal field. Getting back to the charge transfer ex-
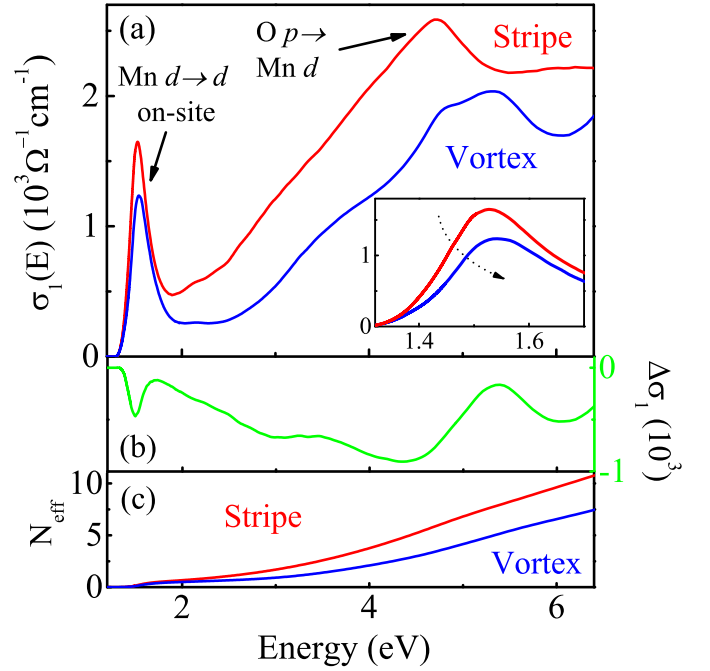

FIG. 4: (a) Optical conductivity of stripe and vortex ErMnO$_3$ in the ab plane at 300 K. Inset: a close-up view of 1.6 eV Mn $d \rightarrow d$ on-site excitation of stripe and vortex ErMnO$_3$. (b) Optical conductivity difference spectrum: $\Delta\sigma_1 = \sigma_{1,vortex} - \sigma_{1,stripe} = \sigma_{1,wall}$. (c) Effective number of electrons involved in the excitations, N_{eff}, as a function of energy.

citations, the spectra reveal that increased domain wall density changes the charge gap and splits one of the O $p \rightarrow$ Mn d charge transfer excitations in ErMnO$_3$. Plots of $(\alpha \cdot E)^2$ vs. energy show that the direct gap shifts from 2.5 eV in the stripe-containing material to 3.1 eV in the vortex sample. The large 0.6 eV shift is a direct consequence of reduced hybridization. This finding suggests that domain wall density can be used to control the band gap - a result that will impact light harvesting with ferroelectric oxides [36]. To assess the strength of the optical excitations, we again calculate the effective number of electrons involved in each transition from the partial sum rule on $\sigma_1(E)$ (Fig. 4(c)). N_{eff} is small below 1.5 eV and grows when the Mn $d \rightarrow$ Mn d excitations begin to contribute [31–33]. At higher energies, N_{eff} is overall larger in the stripe-containing crystal. The oscillator strength difference is a direct consequence of the blue shifted optical excitations in the vortex material. This finding is in line with the expectation that extra wall density leads to increased ionicity and a smaller optical matrix element. We therefore uncover an additional signature of hybridization in ErMnO$_3$ that is consistent with our analysis of the phonons and f manifold excitations.

To summarize, we investigated the spectroscopic response of stripe- and vortex-containing hexagonal ErMnO$_3$ in order to uncover the electronic properties

of the structural domain walls. Analysis reveals enhanced Born effective charge and polarization, identical rare earth environments, and blue shifts of the charge gap with increasing wall density. We bring these findings together with a discussion of hybridization and domain wall density effects, the former of which emanates from the modified local structure of the domain walls as compared to the bulk. Domain wall engineering clearly offers unique prospects for controlling functionality in rare earth manganites like $ErMnO_3$. Similar mechanisms may tune chemical bonding and polarization in other multi-functional oxides and chalcogenides like $IrTe_2$, where the electronic properties correlate with metastable domain wall patterns [37].

†Current address: Department of Chemical and Biological Engineering, University of Colorado, Boulder, Colorado 80309, USA

⊥Current address: Department of Physics and IPAP, Yonsei University, Seoul 120-749, Republic of Korea

[1] J. Seidel *et al.*, Nat. Mater. **8**, 229 (2009).
[2] Y. Wang, C. Nelson, A. Melville, B. Winchester, S. Shang, Z.-K. Liu, D. G. Schlom, X. Pan, and L.-Q. Chen, Phys. Rev. Lett. **110**, 267601 (2013).
[3] M. Fiebig, T. Lottermoser, D. Frohlich, A. V. Goltsev, and R. V. Pisarev, Nature **419**, 818 (2002).
[4] S. C. Chae, Y. Horibe, D. Y. Jeong, S. Rodan, N. Lee, and S. W. Cheong, Proc. Natl. Acad. Sci. U.S.A. **107**, 21366 (2010).
[5] T. Jungk, A. Hoffmann, M. Fiebig, and E. Soergel, Appl. Phys. Lett. **97**, 012904 (2010).
[6] Y. Geng, N. Lee, Y. J. Choi, S. W. Cheong, and W. Wu, Nano Lett. **12**, 6055 (2012).
[7] S. C. Chae, N. Lee, Y. Horibe, M. Tanimura, S. Mori, B. Gao, S. Carr, and S. W. Cheong, Phys. Rev. Lett. **108**, 167603 (2012).
[8] W. Wu, Y. Horibe, N. Lee, S. W. Cheong, and J. R. Guest, Phys. Rev. Lett. **108**, 077203 (2012).
[9] D. Meier, J. Seidel, A. Cano, K. Delaney, Y. Yumagai, M. Mostovoy, N. A. Spaldin, R. Ramesh, and M. Fiebig, Nat. Mater. **11**, 284 (2012).
[10] S. C. Chae, Y. Horibe, D. Y. Jeong, N. Lee, K. Iida, M. Tanimura, and S. W. Cheong, Phys. Rev. Lett. **110**, 167601 (2013).
[11] M.-G. Han, Y. Zhu, L. Wu, T. Aoki, V. Volkov, X. Wang, S. C. Chae, Y. S. Oh, and S.-W. Cheong, Adv. Mater. **25**, 2415 (2013).
[12] Y. Geng, H. Das, A. L. Wysocki, X. Wang, S. -W. Cheong, M. Mostovoy, C. J. Fennie, and W. Wu, Nature Mater. **13**, 163 (2014).
[13] $(\alpha^+\text{-}\beta^-\text{-}\gamma^+\text{-}\alpha^-\text{-}\beta^+\text{-}\gamma^-)$ or $(\alpha^+\text{-}\gamma^-\text{-}\beta^+\text{-}\alpha^-\text{-}\gamma^+\text{-}\beta^-)$
[14] C. J. Fennie and K. M. Rabe, Phys. Rev. B **72**, 100103(R) (2005).
[15] Y. Kumagai and N. A. Spaldin, Nat. Commun. **4**, 1540 (2013).
[16] S. Artyukhin, K. T. Delaney, N. A. Spaldin, and M. Mostovoy, Nat. Mater. **13**, 42 (2014).
[17] Y. Aikawa, T. Katsufuji, T. Arima, and K. Kato, Phys. Rev. B. **71**, 184418 (2005).
[18] Ferroelectric switching is linked to domain wall motion [11, 15].
[19] F. Yen, C. R. dela Cruz, B. Lorenz, E. Galstyan, Y. Y. Sun, C. W. Chu, and M. M. Gospodinov, J. Mater. Res. **22**, 2163 (2007).
[20] L. Kovacs, K. Lengyel, and M. Gospodinov, Mater. Res. Bull. **46**, 2567 (2011).
[21] A. N. Morozovska, E. A. Eliseev, M. D. Glinchuk, L. -Q. Chen, S. V. Kalinin, and V. Gopalan, Ferroelectrics **438**, 32 (2012).
[22] I. Cabrera *et al.*, Phys. Rev. Lett. **103**, 087201 (2009).
[23] E. B. Lochocki, S. Park, N. Lee, S. W. Cheong, and W. Wu, Appl. Phys. Lett. **99**, 232901 (2011).
[24] See Supplemental Material at [URL will be inserted by publisher] for details on growth and characterization.
[25] Domain wall density can be estimated from the AFM images. There are 4 walls in Fig. 1(a), and the length of a typical stripe is 1 mm [4]. Domain wall density is then $n_{stripe} = 4$ walls/[1 mm wall length · 0.025 mm image width] = 160 walls/mm² $\approx$ 200 walls/mm². There are $\approx$1200 walls in Fig. 1(b). $n_{vortex} = 1200$ domain walls/[0.03 mm image size]² $= 1.3 \times 10^6$ domain walls/mm² $\approx 10^6$ domain walls/mm². These are surface densities, but the domains (and their walls) are three-dimensional and go all the way through the crystal [4]. Volume densities can be estimated as $\approx$200 and 10^6 domain walls/mm³ for stripe and vortex, respectively.
[26] J. Vermette, S. Jandl, M. Orlita, and M. M. Gospodinov, Phys. Rev. B **85**, 134445 (2012).
[27] B. B. Van Aken, A. Meetsma and T. T. M. Palstra, Acta Crystallogr. Sect. E: Struct. Rep. Online **57**, i38 (2001).
[28] R. Resta, M. Posternak, and A. Baldereschi, Phys. Rev. Lett. **70**, 1010 (1993).
[29] F. Auzel, Chem. Rev. **104**, 139 (2004).
[30] P. A. M. Dirac, Proc. R. Soc. Lond. A **114**, 243 (1927).
[31] H. J. Xiang, S.-H. Wei, M. H. Whangbo, and J. L. F. Da Silva, Phys. Rev. Lett. **101**, 037209.
[32] W. S. Choi *et al.*, Phys. Rev. B **77**, 045137 (2008).
[33] A. B. Souchkov, J. R. Simpson, M. Quijada, H. Ishibashi, N. Hur, J. S. Ahn, S. W. Cheong, A. J. Millis, and H. D. Drew, Phys. Rev. Lett. **91**, 027203 (2003).
[34] That the TO frequencies are the same is good evidence that the oxygen content is under control.
[35] F. A. C Cotton, *Chemical Applications of Group Theory* (Wiley-Interscience, New York, 1990).
[36] A. Bhatnagar, A. R. Chaudhuri, Y. H. Kim, D. Hesse, and M. Alexe, Nat. Commun. **4**, 2835 (2013).
[37] D. Mazumdar, K. Haule, J. J. Yang, G. L. Pascut, B. S. Hollinsworth, K. R. O'Neal, V. Kiryukhin, S. -W. Cheong, and J. L. Musfeldt, submitted, Phys. Rev. Lett.